

2002

Modelling of particle breakage of coarse aggregates incorporating strength and dilatancy

Buddhima Indraratna

University of Wollongong, buddhima_indraratna@uow.edu.au

W. Salim

University of Wollongong

Publication Details

This article was originally published as Indraratna, B and Salim, W, Modelling of Particle Breakage of Coarse Aggregates Incorporating Strength and Dilatancy, Geotechnical Engineering, Proceedings of Institute of Civil Engineers, 155(4), 2002, 243-252.



Buddhima Indraratna
 Professor of Civil Engineering,
 University of Wollongong,
 NSW, Australia



Wadud Salim
 Doctoral Student, Faculty of
 Engineering, University of
 Wollongong, NSW, Australia



Modelling of particle breakage of coarse aggregates incorporating strength and dilatancy

B. Indraratna and W. Salim

The degradation of coarse aggregates under shear stresses and its influence on the shear strength is studied, considering the energy consumption by particle breakage during shearing. An analytical model is developed relating the deviator stress ratio, dilatancy, friction angle and particle breakage under triaxial loading. Large-scale triaxial testing of latite basalt has been conducted, and the extent of particle breakage during shearing has been quantified. The breakage of particles under monotonic triaxial loading has been considered within the scope of this paper, and the modelling of particle breakage of aggregates under cyclic loading will be presented in a follow-up paper. The results show that the breakage of particles continues to increase beyond the peak deviator stress. The energy consumption by particle breakage is non-linearly related to the particle breakage index. The model also evaluates the effect of particle breakage on the friction angle of ballast. This study sheds further light on the basic angle of friction, which is independent of the breakage of particles during shearing.

NOTATION

B_g	particle breakage index
dE_B	infinitesimal increment corresponding to δE_B
dx_i	infinitesimal increment corresponding to δx_i
dy_i	infinitesimal increment corresponding to δy_i
$d\varepsilon_1$	infinitesimal increment of major principal strain
$d\varepsilon_v$	infinitesimal increment of volumetric strain
F_{1i}	vertical force acting between two particles at contact i
F_{3i}	horizontal force acting between two particles at contact i
M	critical state friction ratio
N_i	normal force between two particles at contact i acting normal to the slip direction
n_1	number of contacts in aggregate per unit length in the direction of σ'_1
n_2	number of contacts in aggregate per unit length in the direction of σ'_2
n_3	number of contacts in aggregate per unit length in the direction of σ'_3
p'	mean effective stress
q	deviator stress
S_i	shear resistance between two particles at contact i

W_{ki}	percentage retained by weight in each grain size fraction before test
W_{kf}	percentage retained by weight in each grain size fraction after test
β_i	angle of slip plane with the direction of major principal stress σ'_1 at contact i
β_c	value of β_i for minimum energy ratio
ΔW_k	difference between W_{ki} and W_{kf}
δE_B	incremental energy consumed due to particle breakage during shearing in a unit volume of aggregate
δE_{bi}	incremental energy consumed due to particle breakage during sliding between two particles at contact i
δu_i	incremental displacement between two particles along slip plane at contact i
δx_i	horizontal component of δu_i
δy_i	vertical component of δu_i
$\delta \varepsilon_1$	finite increment of major principal strain
σ'_1	major principal stress
σ'_2	intermediate principal stress
σ'_3	minor principal stress
ϕ_{cv}	friction angle of an aggregate at constant volume
ϕ_{cs}	friction angle of an aggregate at critical state
ϕ_f	basic friction angle of an aggregate excluding particle breakage and dilatancy effects
ϕ_{fb}	apparent friction angle excluding dilatancy effect but including particle breakage effect
ϕ_{max}	friction angle of an aggregate at maximum deviator stress
ϕ_p	friction angle of an aggregate at peak deviator stress
ϕ_μ	interparticle friction angle between two particles

1. INTRODUCTION

The degradation of aggregates during shearing has always been a concern for researchers and engineers, and especially in the construction and maintenance of high rockfill dams, unbound roads and rail tracks. Limited research is found in the literature regarding the particle breakage of coarse granular aggregates during shearing, or degradation modelling, either analytical or numerical. Although granular aggregates are subjected to cyclic loading in unbound roads and rail tracks, the study of particle breakage and its effects on the shear strength of aggregates under monotonic triaxial loading would improve our insight into and understanding of the behaviour of aggregates under complex cyclic loading. Within the scope of

this paper, the authors have developed an analytical model of particle breakage of coarse aggregates (latite basalt) under a monotonic triaxial loading condition. The model may still be applied in rail track engineering, where the analysis corresponds to the first-stage loading of a repeated (cyclic) loading scheme typically applied by the passage of a train on a rail-ballast track. The authors are in the process of extending the current model to incorporate cyclic loading, so that the degradation of coarse aggregates can be modelled after numerous cycles of repeated loading. The extended model will be published in a follow-up paper.

Many researchers consider the shear strength of granular materials, and particularly of sand, to be dependent upon the basic friction angle and dilatancy during shearing.^{1,2} It is shown that the shear strength increases with increasing dilatancy, which tends to decrease with increasing confining pressure. Lee and Seed³ demonstrated that, under high pressure, the shear strength of sand increased while the dilatancy decreased. They attributed this observation to particle crushing and rearrangement during shearing. Miura and O-hara⁴ indicated that particle breakage could be significant for low-strength granular materials such as decomposed granite, even under low confining pressure. McDowell *et al.*⁵ developed a conceptual model of the probability of fracture of particles in an aggregate based on Weibull⁶ statistics of fracture. McDowell *et al.*⁵ and McDowell and Bolton⁷ added a fracture energy term to the original Cam Clay work energy equation.^{8,9} However, they considered the breakage of particles and the fracture energy only for the special case of one-dimensional compression. Indraratna *et al.*¹⁰ developed an empirical relationship between the peak stress ratio, peak friction angle and particle breakage for ballast aggregates. Ueng and Chen¹¹ presented an analytical formulation for peak principal stress ratio (σ'_1/σ'_3) of sand, considering dilatancy and particle breakage during shearing. In this paper, the effect of particle breakage on the shear strength of coarse aggregates is studied, and an analytical model incorporating the deviator stress ratio (q/p'), dilatancy, friction angle and the energy consumption due to particle breakage is developed for general triaxial shearing based on the Mohr-Coulomb friction theory. Laboratory test results are used in conjunction with the analytical model to explain the effects of particle breakage, dilatancy and confining pressure on the strength and friction angle of coarse aggregates.

Various methods have been used in the past to quantify the breakage of particles during shearing. Marsal¹² developed an index for particle breakage, B_g , where the difference (ΔW_k)

between the percentage retained by weight of each grain size fraction before the test (W_{ki}) and after the test (W_{kf}) was plotted against the aperture of the lower sieve corresponding to that fraction. In this technique, the particle breakage index, B_g , is equal to the sum of the positive values of ΔW_k , expressed as a percentage. Hardin¹³ introduced an alternative index for quantifying the total breakage, B_t , whereas Miura and O-hara⁴ used the surface area increment (ΔS) as an indicator of particle breakage. Hardin's total breakage (B_t) parameter is the area between the gradation curves before and after loading up to 0.074 mm particle size, and requires a planimeter for accurate area measurement. The surface area increment, ΔS , as the indicator of particle breakage is also based on mass gradation curves and requires some assumptions for calculating the specific surface area of different particle (sieve) size. Having compared the various alternative methods, the particle breakage index B_g , proposed by Marsal,¹² has been adopted in this study owing to its simplicity and reliability, in order to quantify the degradation of aggregates during shearing.

2. THEORETICAL DEVELOPMENT

Since triaxial testing is one of the most versatile and useful laboratory methods for obtaining strength and deformation parameters of geomaterials, the interparticle forces and the deformations occurring in a cylindrical triaxial specimen have been considered as the basis for developing the stress-strain relationship of coarse aggregates. Fig. 1 shows an axisymmetric triaxial specimen subjected to drained compression loading. The vertical force, F_{1i} , and the horizontal force, F_{3i} , are acting at the contact i between two typical particles, which are sliding relative to each other under the applied loading. The sliding plane makes an angle β_i with the major principal stress, σ'_1 . If N_i and S_i are the normal force and shear resistance respectively, then by resolving the forces F_{1i} and F_{3i} it can be shown that

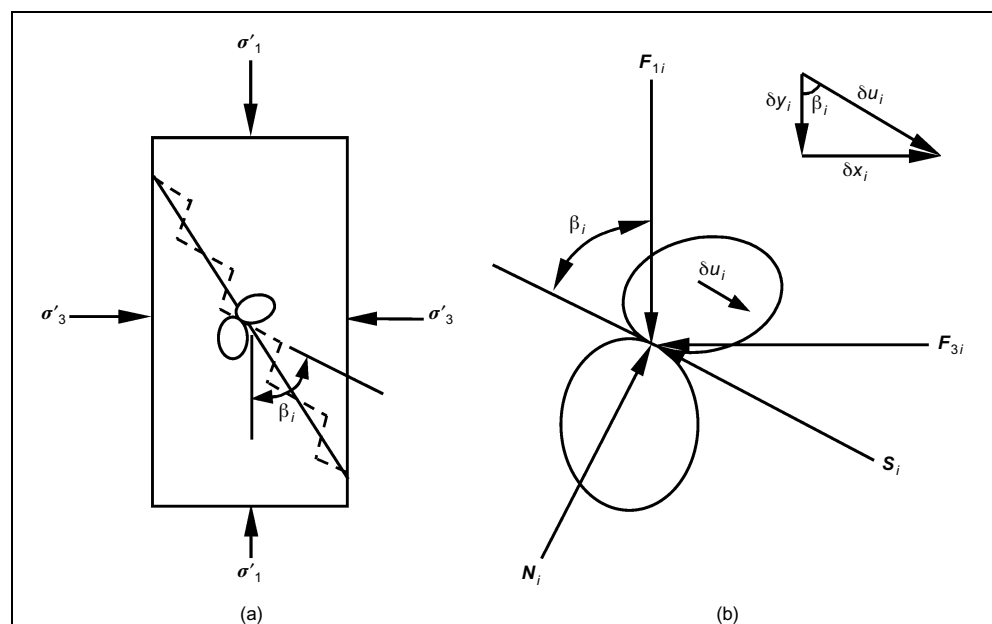


Fig. 1. Triaxial compression test of coarse aggregates (modified after Ueng and Chen¹¹): (a) specimen under stresses and sawtooth deformation model; (b) details of contact forces and deformation at contact of two particles

$$1 \quad N_i = F_{1i} \sin \beta_i + F_{3i} \cos \beta_i$$

$$2 \quad S_i = F_{1i} \cos \beta_i - F_{3i} \sin \beta_i$$

The shear resistance, S_i , can be expressed by the Mohr-Coulomb theory, assuming no cohesion ($c = 0$) between the coarse granular particles. Hence

$$3 \quad S_i = N_i \tan \phi_\mu$$

where ϕ_μ is the friction angle between two particles. If δu_i is the incremental displacement at contact i in the direction of sliding, then the horizontal component δx_i and vertical component δy_i of the displacement δu_i can be expressed by the following relationships

$$4 \quad \delta x_i = \delta u_i \sin \beta_i$$

$$5 \quad \delta y_i = \delta u_i \cos \beta_i$$

$$6 \quad \delta x_i = \delta y_i \tan \beta_i$$

If particle breakage is accompanied with sliding during shearing, then one can assume that the total work done by F_{1i} and F_{3i} at contact i is spent on overcoming frictional resistance and the breakage of particles. Hence

$$7 \quad F_{1i} \delta y_i - F_{3i} \delta x_i = N_i \tan \phi_\mu \delta u_i + \delta E_{bi}$$

where δE_{bi} is the incremental amount of energy spent on particle breakage at contact i during the movement δu_i .

Substituting equations (1), (5) and (6) in equation (7) gives

$$8 \quad F_{1i} \delta y_i - F_{3i} \delta y_i \tan \beta_i = F_{1i} \delta y_i \tan \beta_i \tan \phi_\mu + F_{3i} \delta y_i \tan \phi_\mu + \delta E_{bi}$$

Assuming that n_1 , n_2 and n_3 are the average number of contacts per unit length in the directions of the three principal stresses, σ'_1 , σ'_2 and σ'_3 respectively, the average contact forces and the vertical displacement component can be written as

$$9 \quad F_{1i} = \frac{\sigma'_1}{n_2 n_3}$$

$$10 \quad F_{3i} = \frac{\sigma'_3}{n_1 n_2}$$

$$11 \quad \delta y_i = \frac{\delta \epsilon_1}{n_1}$$

where $\delta \epsilon_1$ is the incremental major principal strain.

Substituting equations (9), (10) and (11) in equation (8), and multiplying both sides by $n_1 n_2 n_3$, gives

$$12 \quad \sigma'_1 \delta \epsilon_1 - \sigma'_3 \delta \epsilon_1 \left(\frac{n_3}{n_1} \right) \tan \beta_i = \sigma'_1 \delta \epsilon_1 \tan \beta_i \tan \phi_\mu + \sigma'_3 \delta \epsilon_1 \left(\frac{n_3}{n_1} \right) \tan \phi_\mu + \delta E_{bi} (n_1 n_2 n_3)$$

where the product $n_1 n_2 n_3$ represents the total number of contacts in a unit volume of granular aggregates. Let $\delta E_B = \delta E_{bi} (n_1 n_2 n_3)$ = incremental energy spent on particle breakage per unit volume of aggregates during the incremental strain $\delta \epsilon_1$, and $r_n = (n_3/n_1)$: then equation (12) becomes

$$13 \quad \sigma'_1 \delta \epsilon_1 - \sigma'_3 \delta \epsilon_1 r_n \tan \beta_i = \sigma'_1 \delta \epsilon_1 \tan \beta_i \tan \phi_\mu + \sigma'_3 \delta \epsilon_1 r_n \tan \phi_\mu + \delta E_B$$

Using the conventional stress parameters p' (mean effective stress) and q (deviator stress), instead of σ'_1 and σ'_3 , equation (13) can be rewritten as follows:

$$14 \quad \left(p' + \frac{2q}{3} \right) \delta \epsilon_1 - \left(p' - \frac{q}{3} \right) \delta \epsilon_1 r_n \tan \beta_i = \left(p' + \frac{2q}{3} \right) \delta \epsilon_1 \tan \beta_i \tan \phi_\mu + \left(p' - \frac{q}{3} \right) \delta \epsilon_1 r_n \tan \phi_\mu + \delta E_B$$

where $p' = (\sigma'_1 + 2\sigma'_3)/3$ and $q = \sigma'_1 - \sigma'_3$.

Rearranging equation (14), the deviator stress ratio becomes

$$15 \quad \frac{q}{p'} = \frac{r_n \tan(\beta_i + \phi_\mu) - 1}{\left[\frac{2}{3} + \frac{1}{3} r_n \tan(\beta_i + \phi_\mu) \right]} + \frac{\delta E_B}{p' \delta \epsilon_1 \left[\frac{2}{3} + \frac{1}{3} r_n \tan(\beta_i + \phi_\mu) \right] [1 - \tan \beta_i \tan \phi_\mu]}$$

In the case of an infinitesimal increment of major principal strain (i.e. $\delta \epsilon_1 \rightarrow 0$), $\delta \epsilon_1$ should be replaced by the differential increment $d\epsilon_1$, and the corresponding increments of δE_B , δy_i and δx_i should be replaced by the differential increments dE_B , dy_i and dx_i respectively. Thus, for the limiting case ($\delta \epsilon_1 \rightarrow 0$), the term $(\delta E_B/\delta \epsilon_1)$ on the right-hand side of equation (15) becomes the derivative $(dE_B/d\epsilon_1)$, and represents the rate of energy consumption due to particle breakage during shearing.

Rowe² suggested that, for granular aggregates, the interparticle friction angle, ϕ_μ , should be replaced by ϕ_f , which is the angle

of friction after correction for dilatancy. The value of ϕ_f varies from ϕ_μ for very dense materials to ϕ_{cv} for very loose materials at constant volume. The difference between ϕ_f and ϕ_μ was attributed to the energy spent on the process of rearrangement of particles during shearing.

According to the minimum energy ratio principle, shear deformation of the aggregate mass will occur when, at each contact i , the energy ratio (ER_i) of the work done by F_{1i} to that by F_{3i} (i.e. $ER_i = F_{1i}\delta y_i / F_{3i}\delta x_i$) is a minimum. By expanding the expression for ER_i and letting $d(ER_i)/d\beta_i = 0$, one can determine the sliding direction at contact i (i.e. $\beta_i = \beta_c$) for the minimum energy ratio condition. In other words, when $ER_i = ER_{\min}$, $\beta_i = \beta_c$. Using this minimum energy ratio principle, Ueng and Chen¹¹ proposed the values of r_n and β_c as given in the following two expressions:

$$16a \quad r_n = \frac{1 - \frac{d\varepsilon_v}{d\varepsilon_1}}{\tan \beta_c}$$

$$16b \quad \beta_c = 45^\circ - \frac{\phi_f}{2}$$

where $d\varepsilon_v$ is the infinitesimal increment of volumetric strain (compression is taken as positive) of the triaxial specimen corresponding to $d\varepsilon_1$.

Substituting equations (16a) and (16b), ϕ_μ by ϕ_f and $\beta_i = \beta_c$ in equation (15), and using the differential incremental terms, the deviator stress ratio becomes

$$17 \quad \frac{q}{p'} = \frac{\left(1 - \frac{d\varepsilon_v}{d\varepsilon_1}\right) \tan^2\left(45^\circ + \frac{\phi_f}{2}\right) - 1}{\left[\frac{2}{3} + \frac{1}{3}\left(1 - \frac{d\varepsilon_v}{d\varepsilon_1}\right) \tan^2\left(45^\circ + \frac{\phi_f}{2}\right)\right]} + \frac{dE_B(1 + \sin \phi_f)}{p' d\varepsilon_1 \left[\frac{2}{3} + \frac{1}{3}\left(1 - \frac{d\varepsilon_v}{d\varepsilon_1}\right) \tan^2\left(45^\circ + \frac{\phi_f}{2}\right)\right]}$$

The quantity $(1 - d\varepsilon_v/d\varepsilon_1)$ represents dilatancy during shearing. In this study, ϕ_f is considered as the basic friction angle of aggregates, which excludes the effects of both dilatancy and particle breakage. The energy consumption due to particle breakage may be related to the particle breakage index B_g (defined earlier) as shown below:

$$18 \quad dE_B = f(dB_g)$$

where dB_g is the differential increment of breakage index corresponding to $d\varepsilon_1$. Combining equations (17) and (18) provides

$$19 \quad \frac{q}{p'} = \frac{\left(1 - \frac{d\varepsilon_v}{d\varepsilon_1}\right) \tan^2\left(45^\circ + \frac{\phi_f}{2}\right) - 1}{\left[\frac{2}{3} + \frac{1}{3}\left(1 - \frac{d\varepsilon_v}{d\varepsilon_1}\right) \tan^2\left(45^\circ + \frac{\phi_f}{2}\right)\right]} + \frac{f(dB_g)(1 + \sin \phi_f)}{p' d\varepsilon_1 \left[\frac{2}{3} + \frac{1}{3}\left(1 - \frac{d\varepsilon_v}{d\varepsilon_1}\right) \tan^2\left(45^\circ + \frac{\phi_f}{2}\right)\right]}$$

The function $f(dB_g)$ in equation (19) remains to be determined based on laboratory triaxial testing.

It is interesting to note that the proposed model simplifies to the critical-state equation when the breakage of particles is ignored. In conventional critical-state soil mechanics,⁹ the breakage of particles during shearing is not taken into consideration. At the critical state, particles will continuously deform at constant stress and constant volume. If the breakage of particles is ignored (i.e. $dE_B = f(dB_g) = 0$) at critical state (i.e. $dp' = dq = d\varepsilon_v = 0$ and $\phi_f = \phi_{cs}$), then equations (17) and (19) are reduced to the following critical state relationships:

$$20 \quad \left(\frac{q}{p'}\right)_{cs} = \frac{\tan^2\left(45^\circ + \frac{\phi_{cs}}{2}\right) - 1}{\frac{2}{3} + \frac{1}{3} \tan^2\left(45^\circ + \frac{\phi_{cs}}{2}\right)} = \frac{6 \sin \phi_{cs}}{3 - \sin \phi_{cs}} = M$$

3. LABORATORY INVESTIGATIONS

Testing of coarse aggregates (at the size of railway ballast) in small (conventional) triaxial equipment can lead to misleading strength–deformation characteristics.¹⁰ It is therefore essential to test such coarse aggregates in a large-scale triaxial apparatus. With this in view, a large-scale triaxial apparatus (Fig. 2) has been designed and built at the University of Wollongong. Several consolidated drained triaxial compression tests were carried out on latite aggregates. The developed model has been applied to the test results to explain the effects of particle breakage, dilatancy and confining pressure on the friction angle of latite basalt.

3.1. Large-scale triaxial apparatus

A large-scale triaxial apparatus (Fig. 2), which can accommodate specimens 300 mm diameter and 600 mm high, was used for investigating the strength–deformation and degradation characteristics of latite basalt. The main components of the apparatus are the triaxial chamber, the axial loading unit, the air pressure and water control unit, the pore water pressure measurement system, the axial deformation measuring device and the volumetric change measurement unit. The volume change of the specimen during consolidation and drained shearing was measured by a coaxial piston located within a small cylindrical chamber (connected to the main cell), in which the smooth piston moves upwards or downwards depending on volume increase or decrease. Further details of the equipment are given elsewhere.^{10,14}

3.2. Material properties

The aggregates tested in this study are crushed volcanic basalt (latite) obtained from a quarry in New South Wales (NSW),



Fig. 2. Large-scale triaxial apparatus built at University of Wollongong, Australia

Australia. The physical properties of latite basalt are given in Table 1. The aggregate crushing value is the ratio of the mass of crushed particles passing a reference sieve to the total mass of aggregate, expressed as a percentage, after being subjected to a specified load (AS 1141.21¹⁵). The Los Angeles abrasion value is the ratio of mass lost due to abrasion (passing a 1.70 mm sieve) to the total mass of aggregate, expressed as a percentage (AS 1141.23¹⁶). The wet attrition value is the ratio of loss of mass (passing a 2.36 mm sieve) to the total mass of aggregate in a wet attrition test (AS 1141.27¹⁷). The point load strength index, $I_{s(50)}$, was determined according to the AS 4133.4.1 method.¹⁸ The uniaxial compressive strength of the parent rock was determined according to the AS 4133.4.2 method.¹⁹ The flakiness index is the percentage by mass of flaky particles, and was measured according to the AS 1141.15 method.²⁰ The proportion of misshapen particles is the

Characteristic test results	Units	Value	Test methods (Australian Standard)
Aggregate crushing value	%	12	AS 1141.21 ¹⁵
Los Angeles abrasion	%	15	AS 1141.23 ¹⁶
Wet attrition	%	8	AS 1141.27 ¹⁷
Point load strength index	MPa	5.39	AS 4133.4.1 ¹⁸
Compressive strength	MPa	130	AS 4133.4.2 ¹⁹
Flakiness Index	%	25	AS 1141.15 ²⁰
Misshapen particles	%	20	AS 1141.14 ²¹

Table 1. Physical characteristics of latite basalt (after Indraratna et al.¹⁰)

percentage of flat, elongated, and flat and elongated particles in an aggregate mass, and was measured according to AS 1141.14.²¹ The grain size distribution of aggregates is presented in Fig. 3. The size of particles varied between 19 mm and 53 mm with a mean size (d_{50}) of 37 mm. The particle size distribution of latite basalt after the test is also shown in Fig. 3 to indicate typical particle degradation.

3.3. Preparation of specimens and test procedure

The specimen was prepared inside a 5 mm thick rubber membrane placed within a split cylindrical mould. Compaction of aggregates was carried out in several layers using a vibratory hammer. The dry unit weight of the specimens varied in the range 15.3–15.4 kN/m³. The corresponding initial void ratio (e_0) was about 0.72. During laboratory compaction, a 4 mm thick rubber pad was used at the tip of the hammer to minimise the risk of breakage of particles during vibration.

After placing the compacted specimen inside the triaxial cell, the cell was filled with water by an upward flow from the bottom plate and left overnight for saturation. Consolidation of the specimen was commenced after achieving the pore pressure parameter, $B > 95\%$. The stress measurements were corrected for the membrane effect as described by Duncan and Seed.²² Fully drained compression tests were conducted at relatively low to moderate confining pressures (10–300 kPa). Ballast in rail track is usually under low confinement produced by the weight of crib ballast, sleeper and track superstructure. However, the stresses generated during maintenance operations (tamping) could be moderate to high values. The range of confining pressures for laboratory investigations was selected to represent the typical ballast confinement in the track. All tests were carried out in this study at an axial strain rate of 0.25%/min, which was sufficiently low to dissipate excess pore pressures developed during shearing. Each specimen was sieved

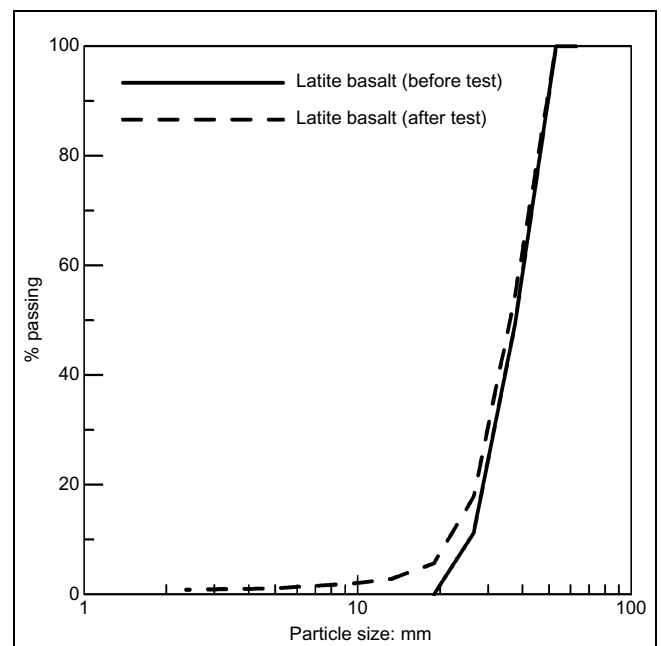


Fig. 3. Grain size distribution of latite aggregates before and after test

before and after the test, and the changes in particle size were recorded to quantify particle breakage.

4. EXPERIMENTAL RESULTS

The latite aggregates were degraded owing to the application of monotonic shear stresses. It is important to note that the stresses applied in this study were sufficiently low compared with the compressive strength (130 MPa) of the parent rock. However, owing to the stress concentrations at the sharp corners and angles, the applied stresses were sufficient to cause breakage of asperities, which is reflected in the change of the particle size distribution curve shown in Fig. 3. Visual inspection of the aggregates recovered after testing confirmed that the degradation process under the current loading scheme was mainly of wear rather than bulk fracture.

The change in particle size (ΔW_k) of aggregates after 20% axial straining in the large-scale triaxial apparatus is shown in Fig. 4 for the two limiting confining pressures (10 kPa and 300 kPa) used in this study. The plots of ΔW_k for the intermediate confining pressures follow a similar trend as in Fig. 4, and are therefore not shown here. Fig. 4 indicates that the change in particle size (ΔW_k) increases with increasing confining pressure, and that larger particles in the range 30–45 mm size (i.e. close to the positive peak) are most vulnerable to degradation.

The breakage indices (B_g) of latite basalt obtained after terminating tests at various axial strains (0%, 5%, 10% and 20%) are plotted in Fig. 5. The failure strains (ϵ_{1f}) are indicated on the plots, and the locus of failure strains is also shown. Here, the failure strain is defined as the axial strain at peak deviator stress. Fig. 5 demonstrates clearly that the degree of particle breakage increases with increasing axial strain, and with higher confining pressure. Particle breakage continues to increase even after the peak deviator stress. The rate of particle

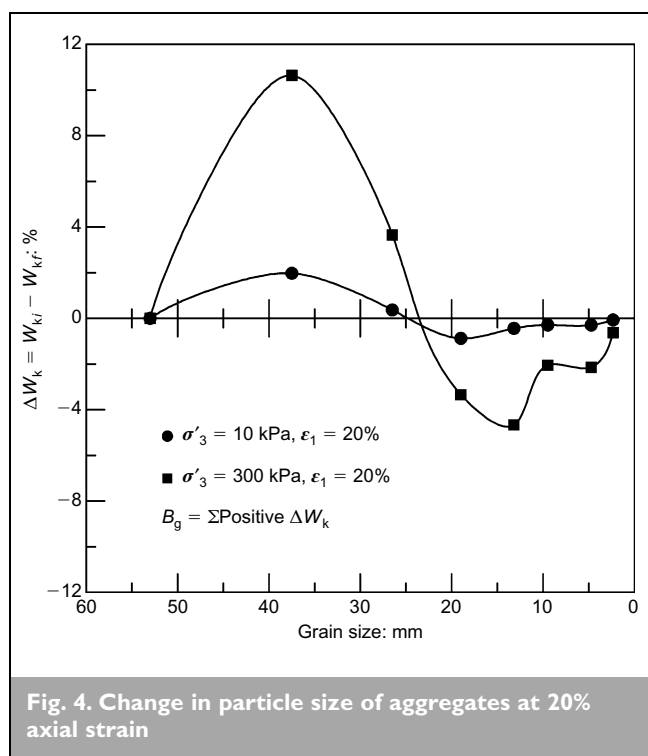


Fig. 4. Change in particle size of aggregates at 20% axial strain

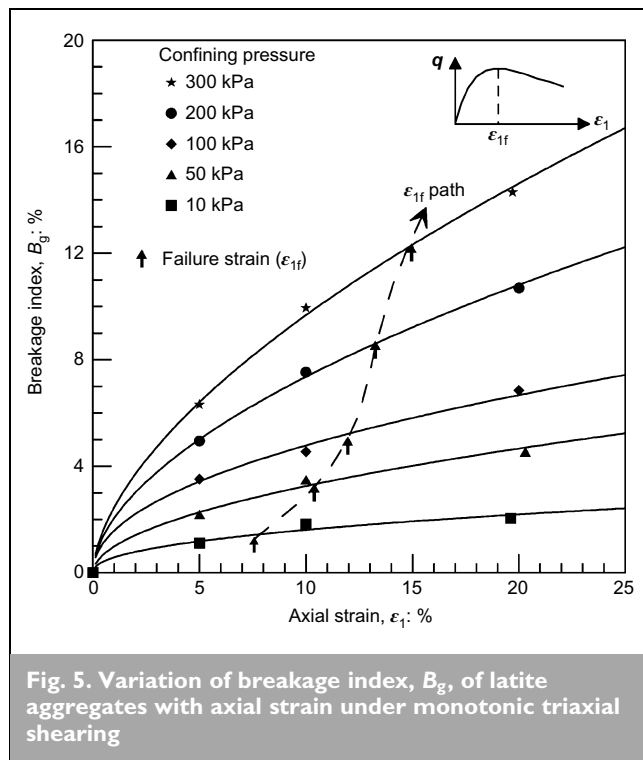


Fig. 5. Variation of breakage index, B_g , of latite aggregates with axial strain under monotonic triaxial shearing

breakage ($dB_g/d\epsilon_1$) decreases with increasing axial strain, but increases with increasing confining pressure.

Figure 6 shows the deviator stress ratio $(q/p)'_f$ against dilatancy $(1 - d\epsilon_v/d\epsilon_1)_f$ at failure. It appears that the stress ratio $(q/p)'_f$ for latite basalt increases slightly non-linearly with dilatancy. The triaxial test data on decomposed granite (sand size) reported by Miura and O-hara⁴ and on Fulung sand presented by Ueng and Chen¹¹ are also plotted in Fig. 6 for comparison, which indicate more linear trends compared with

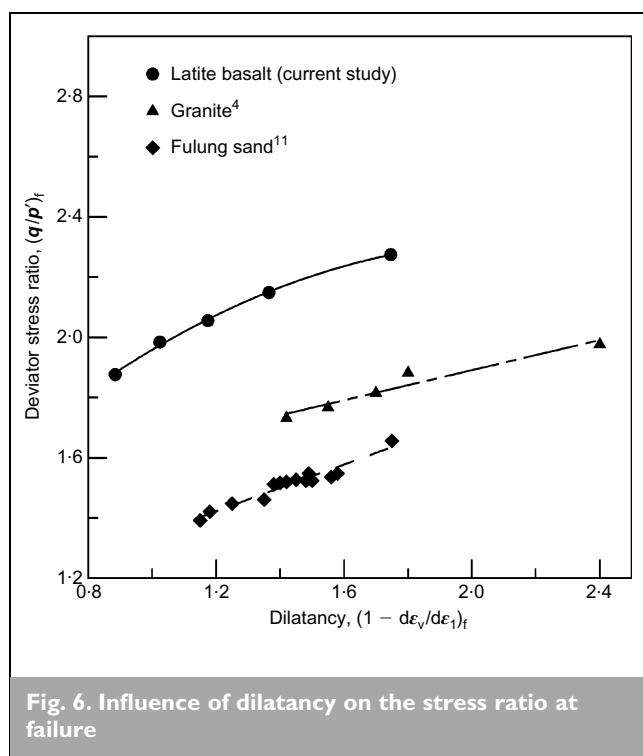


Fig. 6. Influence of dilatancy on the stress ratio at failure

the latite aggregates. The non-linearity of the basalt response is probably due to its much coarser and angular shape than that of the decomposed granite and Fulung sand, hence making it more prone to degradation upon loading.

4.1. Energy consumption during particle breakage

In order to quantify the energy consumption due to particle breakage, the value of the basic friction angle, ϕ_f , in equation (17) needs to be determined first. For the purpose of estimating ϕ_f , the last term of equation (19) containing particle breakage can be set to zero, and the resulting apparent (equivalent) friction angle may be denoted by ϕ_{fb} , which naturally includes the contribution from particle breakage. Thus equation (19) can now be simplified as follows:

$$21 \quad \frac{q}{p'} = \frac{\left(1 - \frac{d\varepsilon_v}{d\varepsilon_1}\right) \tan^2\left(45^\circ + \frac{\phi_{fb}}{2}\right) - 1}{\frac{2}{3} + \frac{1}{3} \left(1 - \frac{d\varepsilon_v}{d\varepsilon_1}\right) \tan^2\left(45^\circ + \frac{\phi_{fb}}{2}\right)}$$

Using the triaxial data of stress ratio $(q/p')_f$ and dilatancy at failure $(1 - d\varepsilon_v/d\varepsilon_1)_f$ in equation (21), the value of ϕ_{fb} can be determined, which includes the contribution from particle breakage but excludes the dilatancy effect. The calculated ϕ_{fb} values are plotted against initial confining pressure in Fig. 7, and against the rate of particle breakage at failure $(dB_g/d\varepsilon_1)_f$ in Fig. 8. It is evident from Fig. 7 that ϕ_{fb} increases at a diminishing rate with increasing confining pressure. At elevated confining pressure, a greater amount of energy is consumed during particle breakage, which is reflected in the increasing value of ϕ_{fb} . A non-linear relationship between ϕ_{fb} and the rate of particle breakage at failure $(dB_g/d\varepsilon_1)_f$ is obtained as shown in Fig. 8. By extrapolating this relationship to zero rate of particle breakage (i.e. $(dB_g/d\varepsilon_1)_f = 0$), the basic friction angle (ϕ_f) can be estimated. The value of ϕ_f of latite

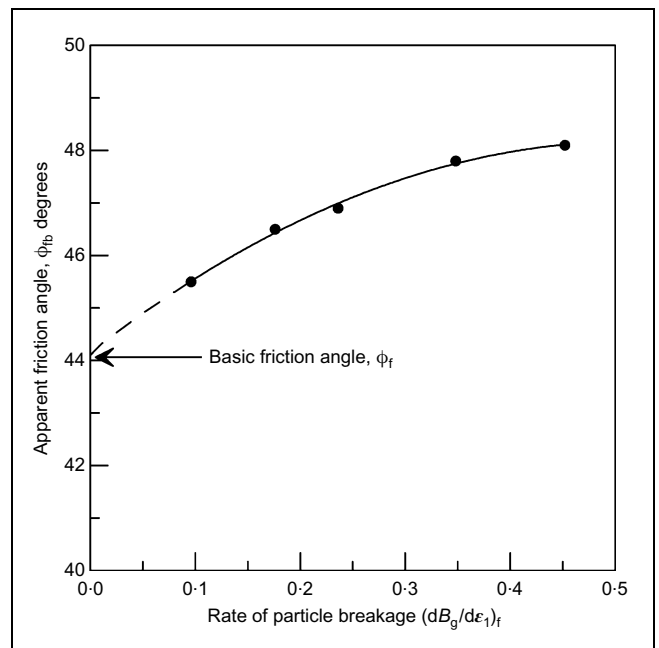


Fig. 8. Variation of ϕ_{fb} with the rate of particle breakage at failure $(dB_g/d\varepsilon_1)_f$

aggregates based on the current triaxial testing is found to be approximately 44° (see Fig. 8).

The rate of energy consumption due to particle breakage at failure $(dE_B/d\varepsilon_1)_f$ can be calculated using equation (17), substituting the above values of ϕ_f , deviator stress ratio $(q/p')_f$ and dilatancy $(1 - d\varepsilon_v/d\varepsilon_1)_f$ at failure. Fig. 9 shows the variations of the rate of energy consumption by particle breakage $(dE_B/d\varepsilon_1)_f$ and the rate of particle breakage at failure $(dB_g/d\varepsilon_1)_f$ with increasing confining pressure. Both $(dB_g/d\varepsilon_1)_f$ and $(dE_B/d\varepsilon_1)_f$ increase with increasing confining pressure. It

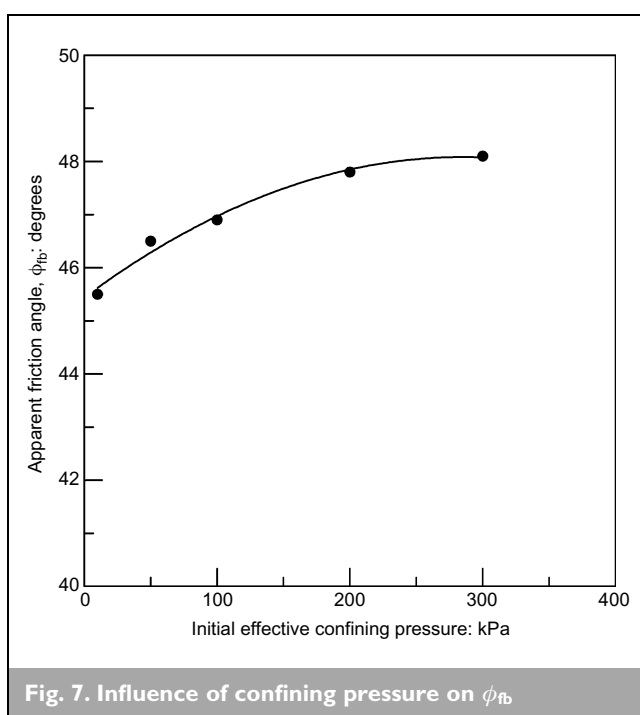


Fig. 7. Influence of confining pressure on ϕ_{fb}

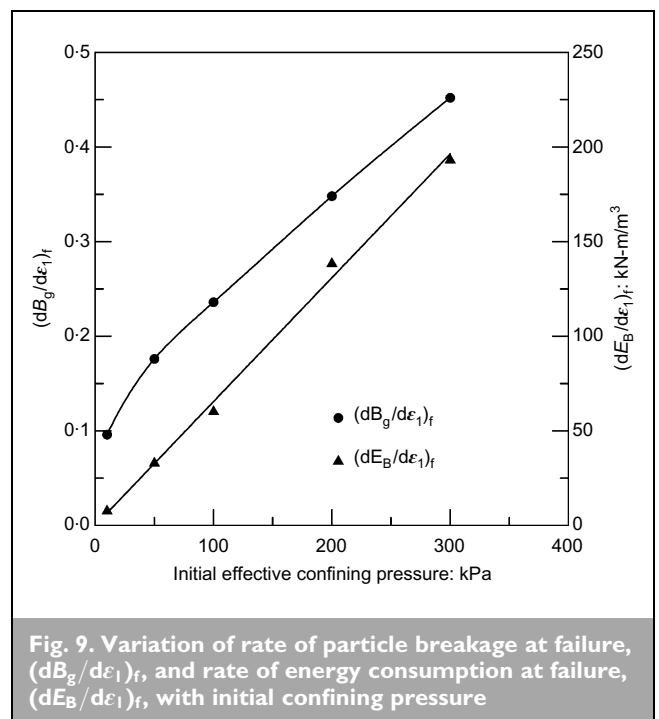


Fig. 9. Variation of rate of particle breakage at failure, $(dB_g/d\varepsilon_1)_f$, and rate of energy consumption at failure, $(dE_B/d\varepsilon_1)_f$, with initial confining pressure

appears in Fig. 10 that the relationship between $(dE_B/d\varepsilon_1)_f$ and $(dB_g/d\varepsilon_1)_f$ can best be represented by a power relationship:

$$22 \quad \left(\frac{dE_B}{d\varepsilon_1}\right)_f = a \left[\left(\frac{dB_g}{d\varepsilon_1}\right)_f\right]^b$$

where a and b are empirical constants. For the latite basalt, $a = 1195$ and $b = 2.12$ have been found from the current data.

4.2. Effect of particle breakage on peak friction angle

By rearranging the Mohr–Coulomb failure criterion, the peak friction angle (ϕ_p) can be conveniently calculated from the following relationship:

$$23 \quad \left(\frac{\sigma'_1}{\sigma'_3}\right)_p = \frac{1 + \sin \phi_p}{1 - \sin \phi_p}$$

The above conventional equation considers the peak principal stress ratio $(\sigma'_1/\sigma'_3)_p$ to determine the peak friction angle, ϕ_p , and hence provides an obvious upper bound for the interparticle friction. The basic friction angle, ϕ_f , evaluated at zero dilatancy and at zero particle breakage provides a lower bound (see Fig. 8), and it is independent of the confining pressure. In this respect, the basic friction angle, ϕ_f , is about the same as the angle of repose of the material. As explained earlier, the apparent friction angle, ϕ_{fb} , includes particle breakage but it is independent of dilatancy.

Figure 11 illustrates the values of various angles of friction with increasing effective confining pressure. At lower confining pressure, the difference between ϕ_p (equation (23)) and ϕ_{fb} (equation (21)) becomes considerable because of the higher dilatancy. At elevated confining pressure, the difference between ϕ_{fb} and ϕ_f increases because of the higher rate of

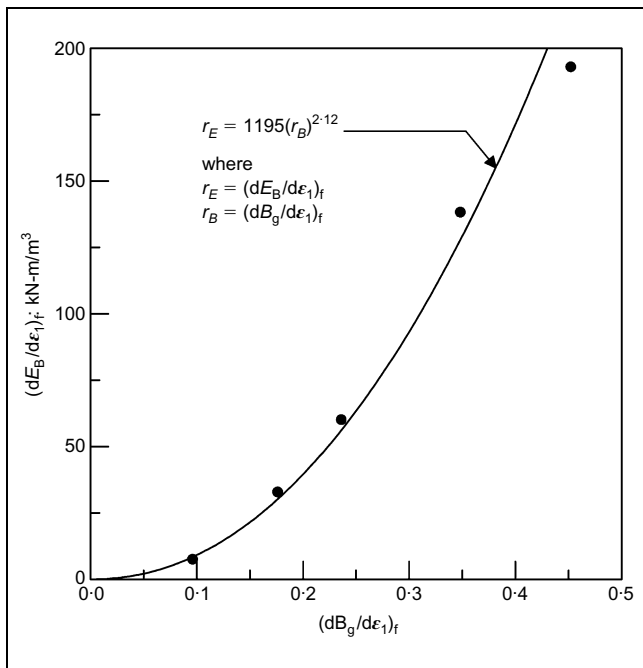


Fig. 10. Rate of energy consumption, $(dE_B/d\varepsilon_1)_f$, against rate of particle breakage, $(dB_g/d\varepsilon_1)_f$

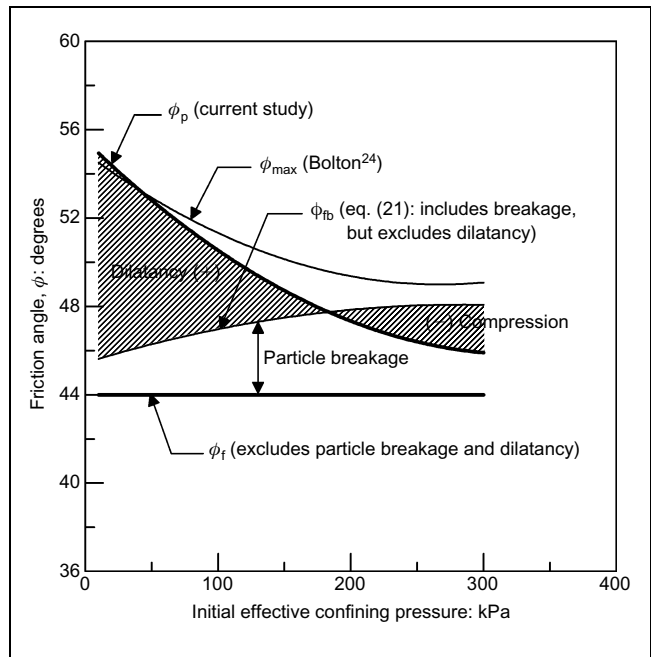


Fig. 11. Effect of particle breakage, dilatancy and confining pressure on the friction angle of latite basalt ($d_{50} = 37.0$ mm)

particle degradation (i.e. increased energy consumption). The peak friction angle, ϕ_p , can therefore be considered as the summation of basic friction angle, ϕ_f , and the effects of dilatancy and particle breakage, as illustrated in Fig. 11. The peak friction angle decreases with increasing confining pressure, and this observation is consistent with previous studies.^{10, 12, 23} Bolton²⁴ modelled the dilatancy-related component of friction angle, $\phi_{max} - \phi_{crit}$, for sand as a function of the relative dilatancy index, which is related to the initial compacted density and the effective mean stress at failure. If the value of ϕ_f derived in Fig. 8 is considered as the value of ϕ_{crit} for the latite aggregates, then the maximum friction angle, ϕ_{max} , can be predicted easily using Bolton's model. The predicted value of ϕ_{max} is obtained by adding the dilatancy component to ϕ_{crit} ; however, the role of particle breakage is not incorporated. While this is realistic for fine granular media such as sand, Bolton's model may not be accurate for coarser and angular aggregates such as latite basalt, for which particle degradation can be significant. Nevertheless, the predicted ϕ_{max} for latite basalt is shown in Fig. 11 for comparison, which reveals that Bolton's model predicts ϕ_{max} for basalt in close agreement to ϕ_p at low confining pressure, where the rate of particle breakage is negligible. However, it seems that Bolton's model overpredicts the maximum friction angle (or dilatancy-related friction component) of coarse aggregates at higher confining pressure. The current model may be used to distinguish clearly the particle breakage component, dilatancy component and basic friction component of the shear strength of angular coarse aggregates.

5. CONCLUSIONS

The degree of particle breakage affects the strength characteristics of coarse aggregates. An analytical model has been developed to include the relationship between the

deviator stress ratio (q/p'), dilatancy, basic friction angle and rate of energy consumption due to particle breakage. Laboratory investigations have been conducted on latite aggregates using a large-scale triaxial apparatus, and the breakage of particles during shearing has been quantified. The results indicate that the apparent friction angle, ϕ_{fb} (which includes particle breakage, but excludes dilatancy effect), increases at a decreasing rate with the higher confining pressure and with the rate of particle breakage. The basic friction angle, ϕ_f , has been estimated as the value of ϕ_{fb} at zero rate of particle breakage, and is found to be about 44° for the latite aggregates used in this study. The analytical model has been applied to the test results, and it is shown to be useful in explaining the effects of dilatancy and particle degradation on the variation of friction angle with confining pressures. The findings of this study confirm that the peak friction angle, ϕ_p , is the summation of basic friction angle, ϕ_f , and the effects of dilatancy and particle breakage during shearing.

The test results verify that the breakage of aggregates increases with increasing confining pressure, and that the larger aggregates are more vulnerable to degradation. Particle breakage increases with axial strain at a decreasing rate, and continues to increase even after the peak deviator stress. The stress ratio of latite basalt increases slightly non-linearly with dilatancy, and this response may be attributed to the increasing vulnerability of coarser aggregates to degradation upon loading. The rate of energy consumption $(dE_B/d\epsilon_1)_f$ is best represented by a power relationship with the rate of particle breakage $(dB_g/d\epsilon_1)_f$ at failure. The current findings show that, at low confining pressure, latite aggregates exhibit a high peak friction angle associated with greater dilatancy. At elevated confining pressure the effect of dilatancy is small, but the increased particle breakage contributes significantly to the frictional behaviour of coarse aggregates.

The degradation of coarse aggregates under static loading provides an important insight into degradation under cyclic loading. This is because the particle breakage taking place under static loading can be considered as the preliminary modelling step of repeated loading. The extent of particle breakage during the first stage of cyclic loading is expected to be comparable to that of static loading. Extension of the current model to cyclic loading is still ongoing, and the authors expect to report these findings at a later date.

6. ACKNOWLEDGEMENTS

The authors wish to express their sincere gratitude and appreciation to the Australian Research Council (ARC) and Rail Infrastructure Corporation (RIC) of NSW, Australia, for supporting this research project. Continued research on this subject area by the Cooperative Research Centre (CRC) for Railway Engineering and Technologies is also acknowledged.

REFERENCES

1. TAYLOR D. W. *Fundamentals of Soil Mechanics*. Wiley, New York, 1948.
2. ROWE P. W. The stress-dilatancy relation for the static equilibrium of an assembly of particles in contact. *Proceedings of the Royal Society of London, Series A*, 1962, 269, 500–527.
3. LEE K. L. and SEED H. B. Drained strength characteristics of sand. *Journal of the Soil Mechanics and Foundations Divisions, ASCE*, 1967, 93, No. SM6, 117–141.
4. MIURA N. and O-HARA S. Particle crushing of decomposed granite soil under shear stresses. *Soils and Foundations*, 1979, 19, No. 3, 1–14.
5. MCDOWELL G. R., BOLTON M. D. and ROBERTSON D. The fractal crushing of granular materials. *Journal of the Mechanics and Physics of Solids*, 1996, 44, No. 12, 2079–2102.
6. WEIBULL W. A statistical distribution function of wide applicability. *Journal of Applied Mechanics*, 1951, 18, 293–297.
7. MCDOWELL G. R. and BOLTON M. D. On the micromechanics of crushable aggregates. *Géotechnique*, 1998, 48, No. 5, 667–679.
8. ROSCOE K. H., SCHOFIELD A. N. and THURAIRAJAH A. Yield of clays in states wetter than critical. *Géotechnique*, 1963, 13, 211–240.
9. SCHOFIELD A. N. and WROTH C. P. *Critical State Soil Mechanics*. McGraw-Hill, London, 1968.
10. INDRARATNA B., IONESCU D. and CHRISTIE H. D. Shear behavior of railway ballast based on large-scale triaxial tests. *Journal of Geotechnical and Geoenvironmental Engineering*, 1998, 124, No. 5, 439–449.
11. UENG T. S. and CHEN T. J. Energy aspects of particle breakage in drained shear of sands. *Géotechnique*, 2000, 50, No. 1, 65–72.
12. MARSAL R. J. Mechanical properties of rockfill. In *Embankment Dam Engineering: Casagrande Volume* (HIRSCHFIELD R. C. and POULOS S. J. (eds)). Wiley, New York, 1973, pp. 109–200.
13. HARDIN B. O. Crushing of soil particles. *Journal of Geotechnical Engineering*, 1985, 111, No. 10, 1177–1192.
14. INDRARATNA B. Large-scale triaxial facility for testing of non-homogeneous materials including rockfill and railway ballast. *Australian Geomechanics*, 1996, 30, 125–126.
15. STANDARDS AUSTRALIA. *Methods for Sampling and Testing Aggregates, Method 21: Aggregate Crushing Value*. Standards Australia, Sydney, NSW, 1997, Australian Standard AS 1141.21.
16. STANDARDS AUSTRALIA. *Methods for Sampling and Testing Aggregates, Method 23: Los Angeles Value*. Standards Australia, Sydney, NSW, 1995, Australian Standard AS 1141.23.
17. STANDARDS AUSTRALIA. *Methods for Sampling and Testing Aggregates, Method 27: Resistance to Wear by Attrition*. Standards Australia, Sydney, NSW, 1995, Australian Standard AS 1141.27.
18. STANDARDS AUSTRALIA. *Methods of Testing Rocks for Engineering Purposes, Method 4.1: Rock Strength Tests—Determination of Point Load Strength Index*. Standards Australia, Sydney, NSW, 1993, Australian Standard AS 4133.4.1.
19. STANDARDS AUSTRALIA. *Methods of Testing Rocks for Engineering Purposes, Method 4.2: Rock Strength Tests—Determination of Uniaxial Compressive Strength*. Standards Australia, Sydney, NSW, 1993, Australian Standard AS 4133.4.2.
20. STANDARDS AUSTRALIA. *Methods for Sampling and Testing Aggregates, Method 15: Flakiness Index*. Standards Australia, Sydney, NSW, 1999, Australian Standard AS 1141.15.

21. STANDARDS AUSTRALIA. *Methods for Sampling and Testing Aggregates, Method 14: Particle Shape, by Proportional Calliper*. Standards Australia, Sydney, NSW, 1995, Australian Standard AS 1141.14.
22. DUNCAN J. M. and SEED H. B. Corrections for strength test data. *Journal of the Soil Mechanics and Foundations Division, ASCE*, 1967, 93, No. 5, 121–137.
23. CHARLES J. A. and WATTS K. S. The influence of confining pressure on the shear strength of compacted rockfill. *Géotechnique*, 1980, 30, No. 4, 353–367.
24. BOLTON M. D. The strength and dilatancy of sands. *Géotechnique*, 1986, 36, No. 1, 65–78.

Please email, fax or post your discussion contributions to the secretary by 1 April 2003: email: mary.henderson@ice.org.uk; fax: +44 (0)20 7799 1325; or post to Mary Henderson, Journals Department, Institution of Civil Engineers, 1–7 Great George Street, London SW1P 3AA.